electronics

MDPI

Article

Design and Performance Verification of A-HFM Signals for Simultaneous Frame Detection, Cell ID Assignment, and Doppler Estimation in AUVs Using Multiple Surface Buoys

Sae-Yong Park [1], Tae-Geon Chung [2] and Tae-Ho Im [1,*]

[1] Department of Information and Communication Engineering, Hoseo University, Asan 31499, Republic of Korea; dyd2634@naver.com
[2] Maritime Research and Development Laboratory, LIG Nex1, Seongnam 13488, Republic of Korea; tae.geon.chung@lignex1.com
* Correspondence: taehoim@hoseo.edu; Tel.: +82-540-9642

Abstract: With the advancement of artificial intelligence, the inference capabilities of Autonomous Underwater Vehicles (AUVs) have significantly improved, leading to growing interest in AUV applications. To ensure reliable operations, the field of underwater communications demands robust schemes that account for AUV mobility and enable the formation of underwater cellular networks. Conventional approaches using Linear Frequency Modulation (LFM) and Zadoff–Chu sequence (ZCS) sequences for frame detection and Cell ID (CID) assignment degrade substantially under severe Doppler conditions. In particular, AUVs experience pronounced Doppler shifts due to their mobility in underwater channels. In this study, we propose a methodology in which distinct Superimposed Adjusted-HFM (SA-HFM) signals are assigned to multiple buoys, allowing AUVs to jointly perform frame detection, CID assignment, and Doppler estimation in challenging underwater environments. To validate the proposed scheme, an ocean experiment was conducted in the East Sea of the Republic of Korea. The results demonstrate that the SA-HFM-based signals successfully achieved frame detection, CID assignment, and Doppler estimation at distances ranging from 500 m to approximately 2 km, even when the AUV moved at speeds of 1.02–1.54 m/s. The experimental results indicate that the proposed approach can offer robust underwater communication and facilitate the deployment of underwater cellular networks for mobile AUV operations.

Keywords: adjusted hyperbolic frequency modulation (A-HFM); CID assignment; Doppler estimation; autonomous underwater vehicles (AUVs); underwater cellular networks

Academic Editor: Paul Mitchell

Received: 14 October 2024
Revised: 21 February 2025
Accepted: 25 February 2025
Published: 27 February 2025

Citation: Park, S.-Y.; Chung, T.-G.; Im, T.-H. Design and Performance Verification of A-HFM Signals for Simultaneous Frame Detection, Cell ID Assignment, and Doppler Estimation in AUVs Using Multiple Surface Buoys. *Electronics* **2025**, *14*, 938. https://doi.org/10.3390/electronics14050938

1. Introduction

Recent advancements in artificial intelligence have significantly enhanced the inferential capabilities of unmanned systems. Consequently, research on the technologies required for constructing unmanned systems is actively progressing. In particular, studies on Unmanned Aerial Vehicles (UAVs) and autonomous vehicles on land and Autonomous Underwater Vehicles (AUVs) and Unmanned Surface Vehicles (USVs) in underwater environments are gaining attention. AUVs and USVs have the advantage of performing military operations or exploration activities underwater without human intervention [1–3].

Underwater acoustic research related to AUVs can be broadly categorized into navigation systems and communication systems. For navigation systems, since Global Positioning Systems (GPS) used on land cannot be utilized underwater, research is being conducted on

operating self-contained navigation systems using methods such as Ultra-short Baseline (USBL) or Doppler Velocity Log (DVL) [4]. In communication systems, research is focusing on network configuration and low-latency and high-reliability communication in underwater environments characterized by limited power supply and harsh communication conditions [5–7]. One of the crucial challenges is establishing a stable underwater cellular network that considers the mobility of AUVs [8]. However, the use of acoustics instead of electromagnetic waves in underwater environments presents various difficulties. The slow speed of sound in water (approximately 1500 m/s) constrains high-speed communication, and the variation in sound velocity with water temperature is also problematic. Additionally, multipath phenomena due to the sea surface and seabed, the resulting narrow coherence bandwidth, and Doppler effects caused by current direction and velocity pose challenges in underwater channels [9]. Designing signals that can overcome these harsh underwater channel conditions is essential for constructing underwater cellular networks.

In terrestrial mobile communications, Long-Term Evolution (LTE) uses about 200 Zadoff–Chu sequences (ZCSs) with excellent autocorrelation properties to assign CIDs [10,11]. However, ZCSs have the disadvantage of performance degradation in environments with severe Doppler effects [12]. In contrast, non-terrestrial communications, proposed as a new methodology for 6G, use base stations such as satellites or UAVs that move at high speeds, resulting in severe Doppler effects. To address this, methodologies using chirp signals with robust characteristics against external interference, such as Linear Frequency Modulation (LFM), have been proposed [13]. In the underwater domain, Generalized-ZCS (G-ZCS) has been proposed to address implementation complexity and reduce signal processing latency [14], while other work has employed multiple LFM chirps (featuring distinct chirp rates or up/down sweeps) to assign multiple CIDs [15].

In underwater acoustic communication, Hyperbolic Frequency Modulation (HFM) signals, similar to LFM, are used. HFM signals have a characteristic where the frequency increases hyperbolically over time, and previous studies have confirmed that HFM is more robust against external interference in underwater acoustic channels compared to LFM. Recent research also includes studies on estimating Doppler effects by concatenating HFM signals [16,17]. Joint techniques that compose signals by superimposing LFM and HFM to perform multiple functions with a single signal are being proposed. The joint technique using LFM and HFM demonstrates robust characteristics in time- and frequency-variant channel environments by superimposing up-sweep and down-sweep signals, enabling frame detection, frame timing synchronization, and Doppler shift estimation [12,18–21].

This paper proposes a method for assigning CIDs by introducing Adjusted-HFM (A-HFM), which adds to the existing functions of Superimposed HFM (frame detection, frame synchronization, and Doppler shift estimation). This method utilizes the ability to assign two-bit information (four cases in total) through the results of each matched filter in frame detection. To verify this, experiments were conducted in the East Sea of South Korea, confirming that CIDs could be distinguished even at a separation distance of about 2 km with the transmitting vessel moving at 1.02–1.54 m/s.

Through this research, we confirmed the performance of the CID assignment method in underwater cellular networks using Superimposed HFM, which is expected to play a crucial role in constructing mobile cellular networks for AUVs in the future. The structure of the paper is as follows: Section 2 describes the methodology and preamble for constructing underwater cellular networks, Section 3 explains the proposed A-HFM, Section 4 details the signal configuration, experimental process, and results of the experiments conducted in the East Sea of South Korea, and Section 5 concludes the paper.

2. Preliminaries

2.1. Underwater Acoustic Channel

Underwater communication can be realized through optical, electromagnetic (radio-frequency), or acoustic modalities [22]. Among these, underwater acoustic communication—examined in this study—has been widely adopted in various applications compared with other approaches. Nevertheless, the underwater channel imposes extremely challenging conditions for data transmission. First, because the absorption coefficient is frequency-dependent, the feasible communication range differs across frequency bands [9]. This frequency dependence can be empirically characterized by Thorp's formula. Another notable attribute of the underwater channel is the slow acoustic propagation speed (approximately 1500 m/s), which gives rise to significant delay spreads; importantly, these delay spreads exhibit time-varying behavior. Furthermore, even a stationary transceiver can experience Doppler shifts owing to ocean currents, necessitating Doppler estimation and compensation at the receiver. As a result, the underwater channel is both time- and frequency-varying, preventing the establishment of standardized channel models akin to those defined by 3GPP (e.g., Extended Pedestrian A [EPA], Extended Vehicular A [EVA], Extended Urban A [EUA]) [23]. To address this lack of representative models, researchers have undertaken ocean experiments under specific conditions to collect channel data. In addition, ray-tracing techniques, such as Bellhop, have been explored to construct underwater channel models.

2.2. Methodology for Underwater Cellular Network Configuration

In underwater environments, acoustic waves are utilized instead of radio waves, necessitating the adaptation of terrestrial network algorithms and topologies to suit the unique characteristics of underwater channels [24]. Underwater acoustic communication networks are primarily categorized into centralized networks and sensor-network-based structures such as ad hoc networks.

Centralized network configurations, often employed in fixed-base networks like underwater seismic and environmental sensor systems, obviate the need for routing technologies, as all communication resources are managed by a central base station. This approach significantly reduces implementation complexity and software requirements at the user equipment (UE) level [25]. Conversely, ad hoc or distributed network topologies present considerable challenges in practical implementation, particularly in the construction of routing tables essential for establishing ad hoc communication structures [26–28].

We assume that the surface buoys maintain connectivity with terrestrial base stations and can accurately estimate synchronization, analogous to the 1 PPS (pulse per second) signal from GPS satellites. Furthermore, we consider a situation akin to terrestrial cellular networks, where frequency resources and cell coverage are configured with distance-dependent power assignment to minimize signal interference (Figure 1).

While terrestrial cellular networks often employ Zadoff–Chu sequences (ZCSs) for their superior autocorrelation properties, it is important to note that their performance degrades in channels affected by Doppler shift, a common phenomenon in underwater environments.

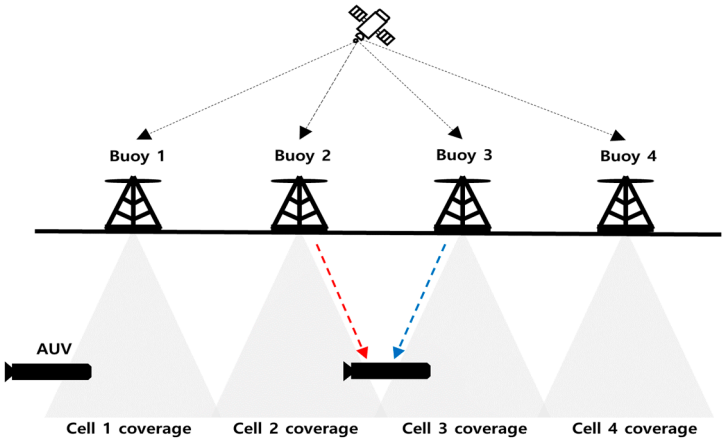

Figure 1. Cellular network using buoys.

2.3. Underwater Communication Preamble

Preambles play a crucial role in underwater acoustic wireless communication by performing pre-synchronization procedures before transmitting data packets. Underwater sensor nodes, being power-sensitive systems, perform preamble detection in the IDLE mode and prepare for reception through frame synchronization detection based on the preamble only when a signal assigned to the sensor node is detected. This addition of preambles to data packets (PDUs) enables smooth communication [29].

The detection probability of preamble signals is critical in the frame synchronization process. Consequently, in harsh underwater channel environments, Linear Frequency Modulation (LFM) and Hyperbolic Frequency Modulation (HFM) are used as preambles due to their robustness against external noise. LFM signals increase frequency linearly over time, while HFM signals have a frequency that increases hyperbolically. In underwater channels, noise effects are typically localized in specific frequency domains. Therefore, LFM and HFM signals, which use a wide frequency range, are less susceptible to noise interference, making them robust in underwater environments [30]. These characteristics also make them suitable for use in side-scan sonar [31–33].

From a communication perspective, LFM and HFM are used as preambles for signal synchronization estimation and Doppler estimation [17,34,35]. Another characteristic of LFM and HFM is that longer signal lengths provide better Signal-to-Noise Ratio (SNR), with HFM exhibiting superior Doppler invariance compared to LFM [36].

Orthogonal Frequency Division Multiplexing (OFDM), which has advantages in high-speed communication and is used as a modulation technique in the physical layer of communication, tends to be sensitive to center frequency offset (CFO) and Synchronization Timing Offset (STO) due to its use of subcarriers [37]. However, in underwater channels, smooth communication throughput performance is challenging due to multipath effects, water currents, and various factors causing Doppler effects. Therefore, if multiple estimations can be made through a single signal, underwater acoustic communication performance can be improved. One technique to enhance this performance is the joint method, which uses Superimposed LFM/HFM to enable frame detection, frame synchronization estimation, and Doppler effect estimation [18,20].

In this paper, we propose an Adjusted-HFM (A-HFM) method by modifying the HFM signal that constitutes the Superimposed HFM, which can improve communication throughput performance. We aim to create a signal that can distinguish CIDs in constructing a cellular network in underwater channel environments by combining this A-HFM with conventional HFM. This approach enables frame detection, frame synchronization estimation, Doppler effect estimation, and CID assignment through the preamble.

3. Superimposed Hyperbolic Frequency Modulation

3.1. Proposed A-HFM

In this paper, we propose an Adjusted-HFM (A-HFM) method, which is a modification of conventional Hyperbolic Frequency Modulation (HFM) known for its robustness against external noise. Conventional HFM, in the case of a down-sweep, refers to a signal that starts at the highest frequency and decreases with a constant chirp rate. This can be expressed as follows:

$$S^{-}_{HFM}(t) = \cos(\frac{2\pi}{b}\ln(bt + \frac{1}{f_{\max}})) \tag{1}$$

$$f^{-}_{HFM}(t) = \frac{1}{\frac{1}{f_{\max}} + bt}. \tag{2}$$

In the case of an up-sweep, the signal starts at the minimum frequency and increases with a constant chirp rate until it reaches the maximum frequency. This can be expressed as follows:

$$S^{+}_{HFM}(t) = \cos(\frac{2\pi}{a}\ln(at + \frac{1}{f_{\min}})) \tag{3}$$

$$f^{+}_{HFM}(t) = \frac{1}{\frac{1}{f_{\min}} + at} \tag{4}$$

$$a = \frac{f_{\min} - f_{\max}}{T_{HFM} f_{\min} f_{\max}} \; b = \frac{f_{\max} - f_{\min}}{T_{HFM} f_{\min} f_{\max}} \tag{5}$$

where S^{-}_{HFM} represents the down-sweep HFM signal in the time domain, f^{-}_{HFM} denotes the frequency component of the down-sweep HFM signal over time, S^{+}_{HFM} represents the up-sweep HFM signal in the time domain, f^{+}_{HFM} denotes the frequency component of the up-sweep HFM signal over time, $f_{\min}$ is the lowest frequency of the HFM signal, $f_{\max}$ is the highest frequency of the HFM signal, and a, b represent the chirp rate of the HFM signal

In this paper, we generate two types of A-HFM signals by applying symmetry and frequency translation to both the down-sweep and up-sweep signals. For the A-HFM down-sweep, we create it by first applying frequency-axis symmetry to the existing up-sweep HFM signal and then translating it parallel by $f_{\min} + f_{\max}$. The equations for the time and frequency domain signals of the generated down-sweep A-HFM are given in Equations (6) and (7), and spectrograms are illustrated in Figure 2a.

$$S^{-}_{A-HFM}(t) = \cos(-\frac{2\pi}{a}\ln(at + \frac{1}{f_{\min}}) + (f_{\min} + f_{\max})t) \tag{6}$$

$$f^{-}_{A-HFM}(t) = -\frac{1}{f_{\min} + at} + (f_{\min} + f_{\max}) \tag{7}$$

where S^{-}_{A-HFM} represents the down-sweep A-HFM signal in the time domain, f^{-}_{A-HFM} denotes the frequency component of the down-sweep A-HFM signal over time, and a, b represent the chirp rate of the A-HFM signal. The second proposed signal, the up-sweep A-HFM, is created by applying y-axis symmetry to the existing down-sweep HFM signal and then translating it parallel by $f_{\min} + f_{\max}$.

The other generated signal, the A-HFM up-sweep, is created by applying y-axis symmetry to the existing down-sweep HFM signal and then translating it parallel by $f_{\min} + f_{\max}$. The equations for the time and frequency domain signals of the generated up-sweep A-HFM are given in Equations (8) and (9), and spectrograms are illustrated in Figure 2b.

$$S^{+}_{A-HFM}(t) = \cos(-\frac{2\pi}{b}\ln(bt + \frac{1}{f_{\max}}) + (f_{\min} + f_{\max})t) \tag{8}$$

$$f^{+}_{A-HFM}(t) = -\frac{1}{f_{\max} + bt} + (f_{\min} + f_{\max}). \tag{9}$$

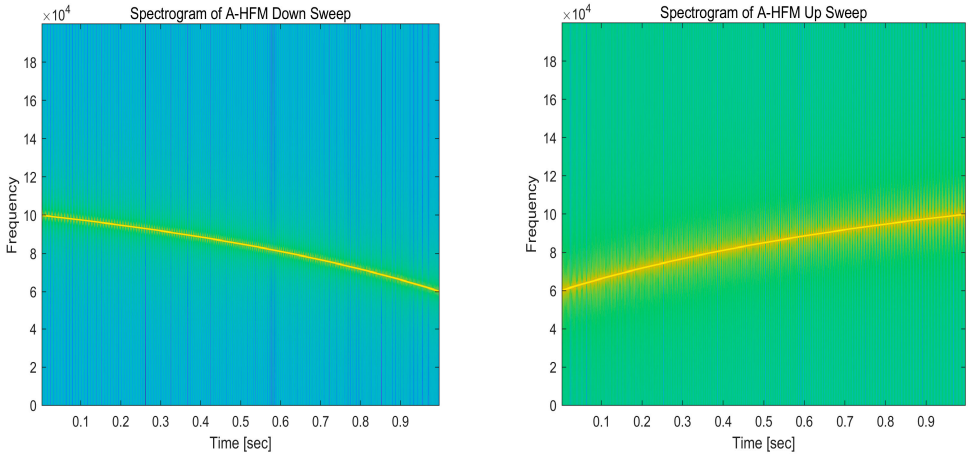

(**a**) (**b**)

Figure 2. Time domain signal and spectrogram of the down- and up-sweep A-HFM signals: (**a**) spectrogram of the down-sweep A-HFM signal, showing the frequency decreasing from 100 kHz to 80 kHz over time; (**b**) spectrogram of the up-sweep A-HFM signal, showing the frequency increasing from 80 kHz to 100 kHz over time.

3.2. Proposed Adjusted-HFM Based on the Superimposed HFM Method

In this paper, we propose the Adjusted-HFM (A-HFM) method based on the Superimposed HFM technique, which is a modification of the conventional HFM known for its robustness against external noise. The Superimposed HFM is an algorithm that enables frame synchronization estimation and Doppler estimation by overlapping different HFM signals. This technique secures time resources for transmitting data packets in unstable environments where high-speed communication is impossible due to the low acoustic wave shear velocity, multipath effects, and physical characteristics of underwater environments.

To generate the A-HFM-based Superimposed HFM signal (SA-HFM) proposed in this paper, we use the following equations:

$$S_{SA-HFM1}(t) = \frac{S^{-}_{HFM}(t) + S^{+}_{HFM}(t)}{2} \tag{10}$$

$$S_{SA-HFM2}(t) = \frac{S^{-}_{A-HFM}(t) + S^{+}_{A-HFM}(t)}{2} \tag{11}$$

$$S_{SA-HFM3}(t) = \frac{S^{-}_{HFM}(t) + S^{+}_{A-HFM}(t)}{2} \tag{12}$$

$$S_{SA-HFM4}(t) = \frac{S^{-}_{A-HFM}(t) + S^{+}_{HFM}(t)}{2}. \tag{13}$$

The spectrograms of each superimposed signal are shown in Figure 3.

In this paper, we propose transmitting the SA-HFM signal generated as described above as a preamble signal, attached to the front of the data packet. This approach enables frame detection, frame synchronization estimation, Doppler estimation, and CID assignment, which are inherent capabilities of the Superimposed HFM technique. Frame detection is achieved by selecting the sample point where the autocorrelation of each signal is maximized, as shown in Equations (14) and (15):

$$t_1 = \arg\max_{\tau} \int_0^{T_{HFM}} r(t+\tau) S^{+}(t) dt \tag{14}$$

$$t_2 = \arg\max_{\tau} \int_0^{T_{HFM}} r(t+\tau) S^{-}(t) dt. \tag{15}$$

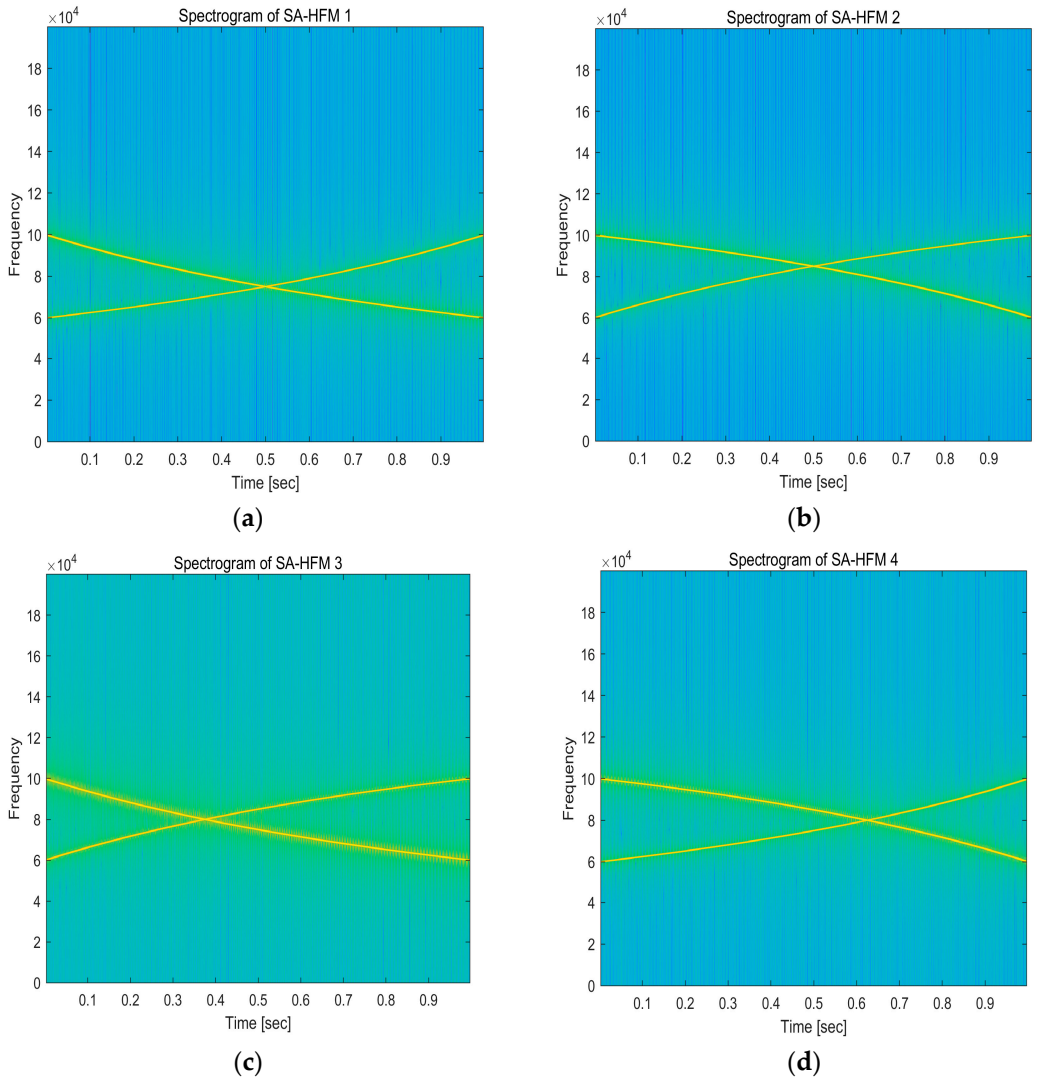

Figure 3. Spectrograms of SA-HFM signals: (**a**) spectrogram of $S_{SA-HFM1}$; (**b**) spectrogram of $S_{SA-HFM2}$; (**c**) spectrogram of $S_{SA-HFM3}$; (**d**) spectrogram of $S_{SA-HFM4}$.

Based on the peak indices detected through Equations (16) and (17), we calculate t_1 and t_2, which represent the differences between the reference peak t_p (the case without any Doppler effect) and the actual HFM signal. The reference peak t_p is the expected peak position in the absence of a Doppler effect. One reason for performing this operation is that HFM signals exhibit a Doppler-invariant property; even if Doppler effects are present, they manifest solely as a shift in the cross-correlation index. For instance, in the case of a down-sweep HFM, a positive Doppler shift causes the correlation peak to appear to the left of the peak for the Doppler-free signal, whereas in an up-sweep HFM, the peak appears to the right of the reference. Equations (16) and (17) leverage this property by computing the difference from the reference peak. The calculations for $\Delta\tau_1$ and $\Delta\tau_2$ are expressed in Equations (16) and (17):

$$\Delta\tau_1 = t_p - t_1 = \frac{T_{HFM} f_{\max} \alpha}{(f_{\max} - f_{\min})(1+\alpha)} \tag{16}$$

$$\Delta\tau_2 = t_p - t_2 = \frac{-T_{HFM} f_{\min} \alpha}{(f_{\max} - f_{\min})(1+\alpha)}. \tag{17}$$

Subsequently, we determine the number of different samples using t_1 and t_2 through Equation (18):

$$\Delta\lambda = f_s(t_2 - t_1) = \frac{f_s T_{HFM} \alpha (f_{\max} + f_{\min})}{(f_{\max} - f_{\min})(1+\alpha)}. \tag{18}$$

The Doppler coefficient can be estimated by substituting t_1, t_2, and $\Delta\lambda$, which are calculated through Equations (12)–(16), into Equation (19):

$$\hat{\alpha} = \frac{(f_{\min} - f_{\max})\Delta\lambda}{f_s T_{HFM}(f_{\max} + f_{\min}) - (f_{\max} - f_{\min})\Delta\lambda}. \tag{19}$$

Subsequently, we can estimate the frame synchronization that shows a discrepancy due to the Doppler effect using Equation (20):

$$\hat{t}_p = \frac{t_1 + \Delta\tau_1 + t_2 + \Delta t_2}{2} + \hat{\alpha} T_{HFM}. \tag{20}$$

Using the above equation, it becomes possible to estimate both the Doppler shift magnitude and the frame synchronization point through cross-correlation of HFM signals that have different sweep directions.

4. Ocean Experiments

4.1. Ocean Experiment Design

In this chapter, we evaluate the performance of frame detection, Doppler estimation, and CID assignment based on sea trials of the proposed Superimposed HFM method. The transmitted signals consisted of four types: tone, LFM, dual HFM, dual A-HFM, and the proposed SA-HFM. The tone signal alone had a duration of 2 s, while the remaining signals each had a duration of 125 ms. In addition, a 500 ms guard interval was inserted between consecutive signals to prevent interference caused by Doppler shifts and multipath propagation.

The inclusion of the tone signal was motivated by the fact that in real maritime environments, velocity estimation errors inevitably arise due to waves, even if the vessel is assumed to move at a constant speed. Since tone signals are extensively employed to estimate Doppler shift and spread, they were used here as a reference for Doppler estimation. We employed the root-mean-square error (RMSE) relative to the tone signal as a performance indicator. Furthermore, to evaluate the CID assignment performance, we compared the CID values assigned to the SA-HFM region using the LFM signal in the collected data as a reference. Furthermore, because the underwater channel environment in question is a doubly dispersive channel—varying over both time and frequency—signals with a center frequency of 15, 20, or 25 kHz and a bandwidth of 4 kHz were transmitted to evaluate the performance across different frequencies. A summary of the remaining experimental signal parameters can be found in Table 1.

Table 1. Ocean experiment signal parameters.

Parameter	Value
Sampling Frequency	200 kHz
Center Frequency	15, 20, 25 kHz
Bandwidth	4 kHz
Signal Duration	125 ms
Guard Interval	500 ms

For the tone signals identified at the receiver, the Doppler shift and Doppler spread were examined using the Fourier transform. In the case of the dual HFM signals created by concatenating HFMs with different sweep directions, we applied the cross-correlation method to detect the peak in the received signal and then performed Doppler estimation. For the proposed SA-HFM, we conducted cross-correlation on the received signal to identify the dominant peaks, after which we assessed the performance of CID assignment by comparing CIDs according to the positions of the designed signals. The transmission procedure is illustrated in Figure 4.

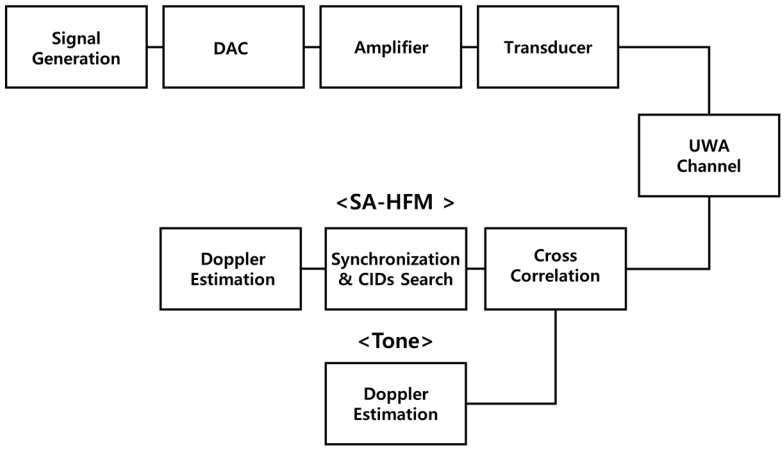

Figure 4. Block diagram of the transmit–receive process used in the ocean experiment.

To evaluate the performance of the preamble between a surface buoy and an AUV in motion, as described in Section 2, we conducted experiments in ocean conditions near 36°28′15.2″ N, 129°35′28.9″ E in the East Sea of the Republic of Korea. In this experimental setup, the vessel serving as the surface buoy was kept stationary, whereas another vessel, acting as the AUV, transmitted signals from sensors positioned at a depth of 100 m. The transmitting vessel traveled at speeds of 1.02–1.54 m/s, and the separation distance between vessels was tracked using a GARMIN GPS 64s (GARMIN, Olathe, KS, USA) under a positioning error of approximately 3 m. The experiments took place over three days, from 24 September to 26 September 2024. We employed a Neptune Sonar D/17/BB transceiver, (Neptune Sonar Ltd., Kelk, UK) for these trials. Because the speed of sound in water is temperature-dependent, which influences the propagation of acoustic rays and can induce multipath effects, we conducted the measurements of the sound speed twice using a Valeport Sound Velocity Profiler (SVP) (TELEDYNE VALEPORT Ltd., Totnes, UK). Figure 5 presents the GPS positions for both the transmitting and receiving vessels, the SVP data obtained, and the instruments employed in the experiment.

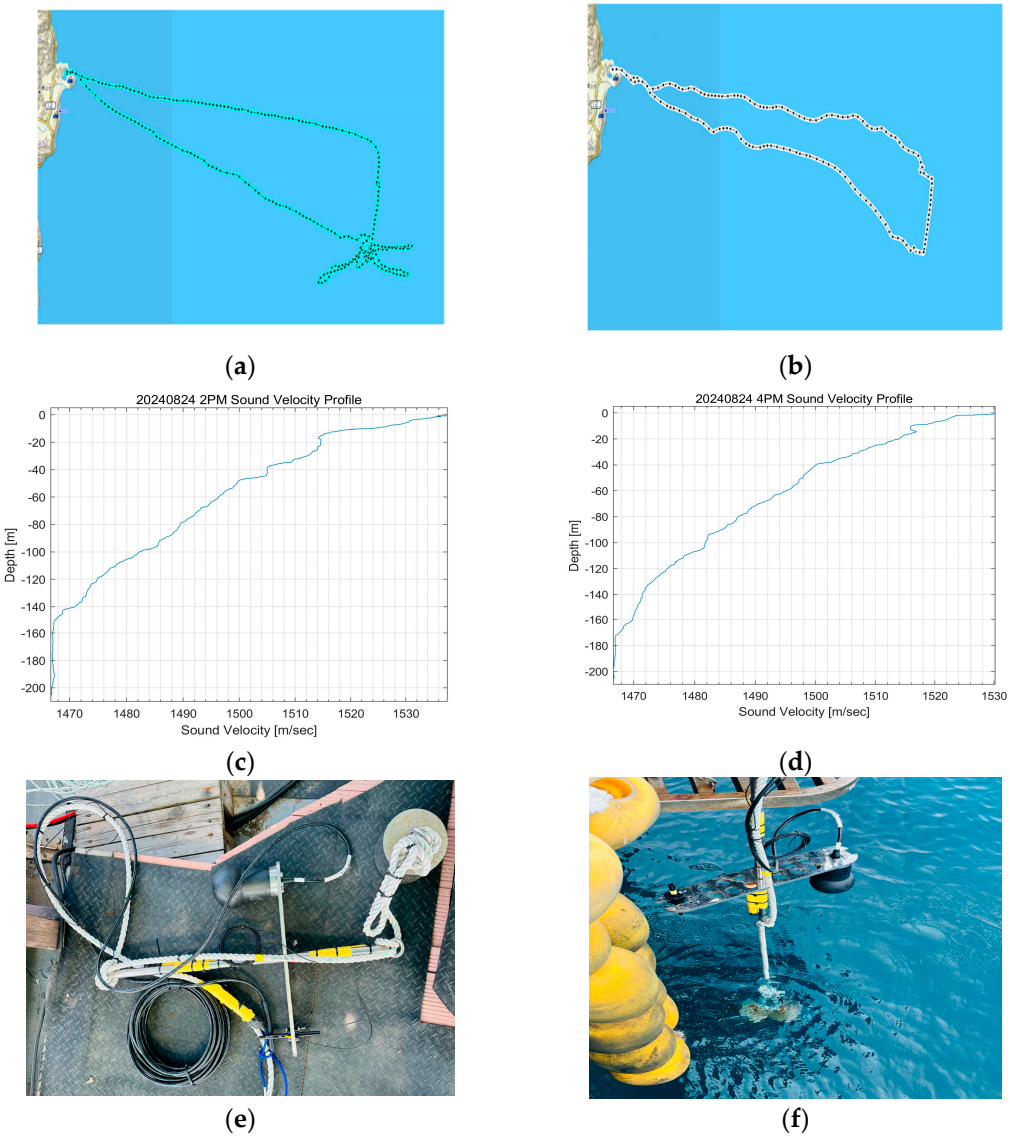

Figure 5. GPS positions of transmitting and receiving vessels, sound velocity profiles, and transceiver sensors on the day of the experiment: (**a**) GPS coordinates of the transmitting vessel. The path diverging into three branches at the 5 o'clock position represents the routes for collecting results at each center frequency; (**b**) GPS coordinates of the receiving vessel, which was anchored during the experiment; (**c**) sound velocity profile at 14:00 on the day of the mobile experiment; (**d**) sound velocity profile at 16:00 on the day of the mobile experiment; (**e**) transceiver sensor 1; (**f**) transceiver sensor 2.

4.2. Result of Ocean Experiment

Unlike simulations, where the channel model is predetermined, this study employed actual ocean experiments in an underwater channel environment that exhibits distinct time- and frequency-varying characteristics, as mentioned in Section 2. To analyze these characteristics, we examined the maximum delay spread induced by the multipath using the power delay profile (PDP) of the HFM signal, and we determined the Doppler shift and spread using both the tone and SA-HFM signals.

First, in the scenario where both the transmitter and receiver vessels were stationary—with the transmitter's transducer at a depth of 100 m and the receiver's hydrophone at a depth of 5 m—the tone-based Doppler shift was estimated to be 0.08 Hz, the SA-HFM-based Doppler shift was 1 Hz, and the maximum delay spread derived from the HFM signal was 4.16 ms. This indicates that even in a stationary underwater channel, Doppler effects do occur, and the 4.16 ms maximum delay spread confirms the influence of the multipath

in the underwater environment. Figure 6a presents the power delay profile (PDP) of the collected signals under the fixed condition, as well as the results for Doppler shift and spread, which are shown in Figure 6.

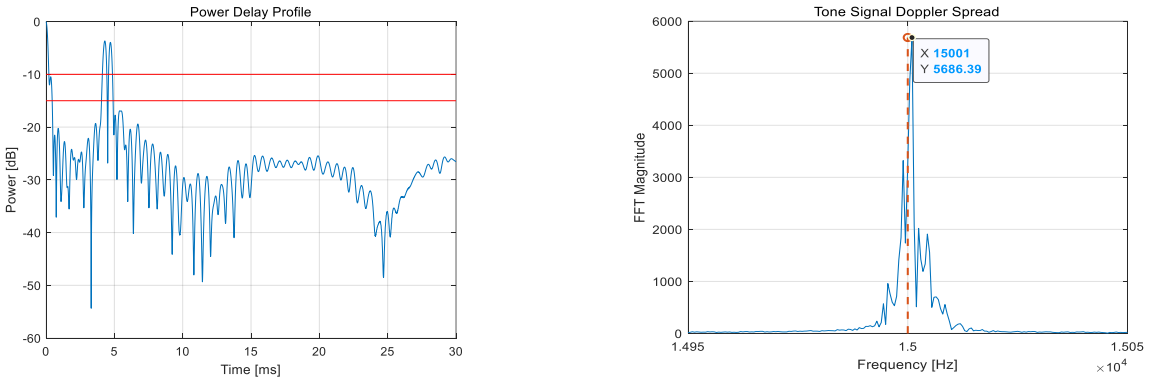

(**a**) (**b**)

Figure 6. Channel characteristics at 15,000 Hz center frequency, 100 m separation distance, transmitting sensor depth of 100 m, and receiving sensor depth of 5 m: (**a**) power delay profile under these conditions; (**b**) Doppler spread based on tone signal.

Next, considering a mobile setting, both the transmitter and receiver sensors were placed at a depth of 100 m. The initial inter-vessel distance of 500 m was extended up to 2200 m, with vessel speeds ranging from 1.02 to 1.54 m/s. For a center frequency of 20 kHz, the average maximum delay spread was estimated at 7.91 ms, while the tone-based Doppler effect was measured at 13.8 Hz and the SA-HFM-based Doppler effect at 12.8 Hz. Comparing these results with the theoretical Doppler shift values in Table 2 indicates that the estimated performance was consistent with vessel speeds of approximately 1.02–1.54 m/s. The close agreement between the Doppler shift estimates using the tone and SA-HFM signals reinforces their reliability. However, in terms of the CID assignment performance of the SA-HFM, three missed detections occurred at 15 kHz, likely due to a low SNR during data collection, as shown in Figure 7e. Specifically, when the SNR dropped below −10 dB, the SA-HFM signal could not be detected.

Table 2. Theoretical Doppler shift values for different center frequencies according to movement speed.

m/s	km/h	Doppler Factor	Doppler Shift (15 kHz)	Doppler Shift (20 kHz)	Doppler Shift (25 kHz)
0	0	0	0	0	0
0.51	1.85	0.000342	5.13	6.84	8.55
1.02	3.70	0.000685	10.27	1370	17.12
1.54	5.55	0.001028	15.42	20.56	25.70
2.05	7.40	0.001371	20.56	27.42	34.27
2.57	9.23	0.001714	25.71	34.28	42.85
3.08	11.11	0.002057	30.85	41.14	51.42
3.60	12.96	0.002407	36.10	48.14	60.17

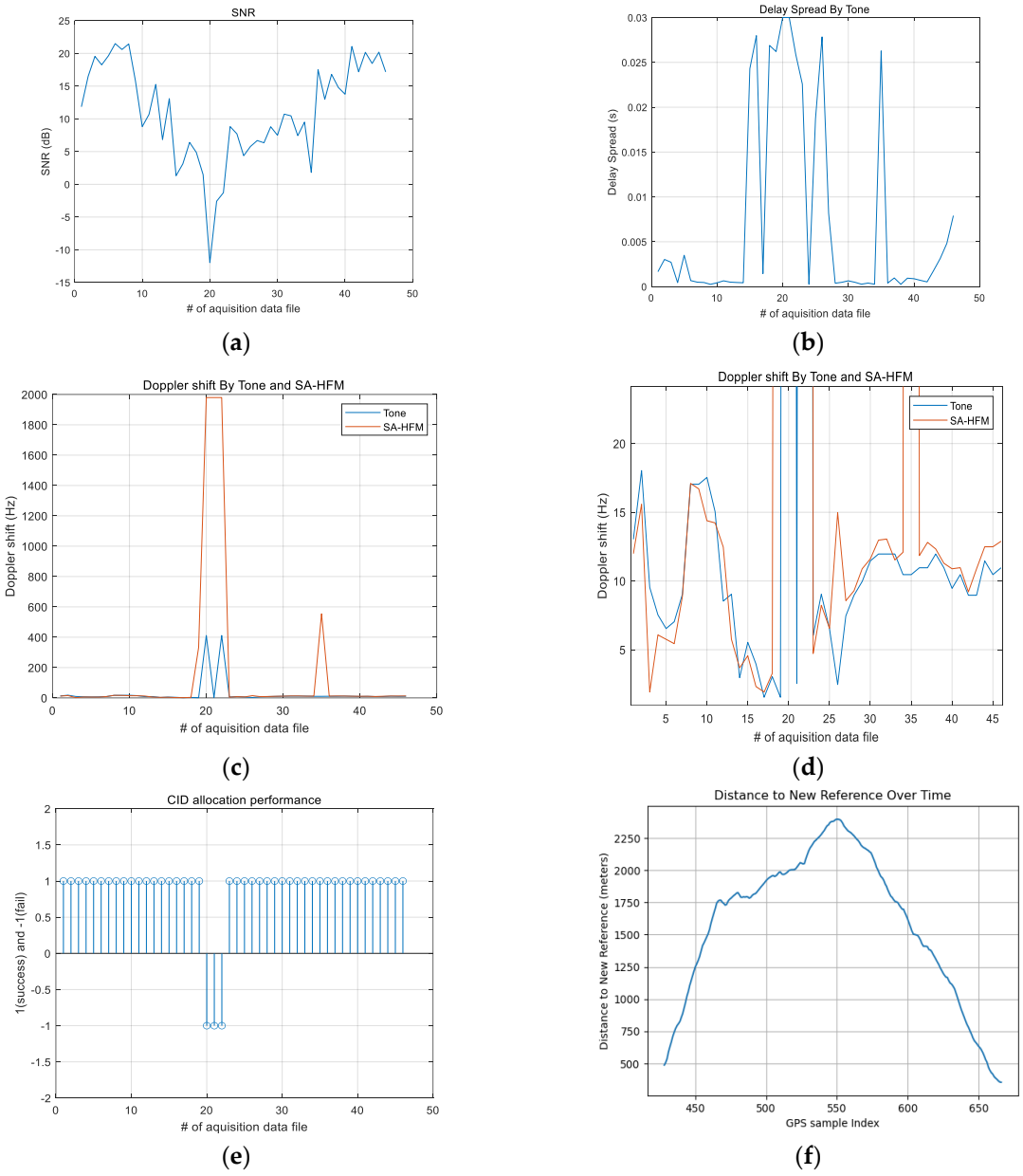

Figure 7. Channel characteristics and CID assignment performance in mobile experiment simulation: (**a**) measured SNR; (**b**) maximum delay spread (**c**) Doppler estimation performance based on SA-HFM; (**d**) Doppler estimation performance based on tone signal; (**e**) CID assignment performance; (**f**) time-dependent separation distance between transmitting and receiving vessels.

The number of collected data points varied for each signal type due to the different experimental conditions. For the mobile experiments, data were collected up to approximately 2 km from the receiving vessel's GPS position, resulting in a larger dataset compared to the other collection scenarios.

Table 3 summarizes the tone-signal-based RMSE for the SA-HFM under the aforementioned conditions. In calculating the RMSE, intervals pertaining to both the tone-based and SA-HFM Doppler shifts were excluded because frame detection was not performed. The results indicate that the RMSE relative to the tone signal used for Doppler estimation remained below approximately 7 Hz and that the CID assignment performance exceeded 90% for all tested signals, except for the 20 kHz signal.

Table 3. Underwater channel characteristics and CID assignment performance results for different center frequencies.

Center Frequency	CID Assignment (%)	RMSE of Doppler Estimation (Hz)
15 kHz	93	2.54
20 kHz	75	7.5
25 kHz	100	2.2

5. Conclusions

In this study, we proposed a novel approach for establishing cellular networks in underwater environments using the Superimposed Adjusted-HFM (SA-HFM) technique. While conventional HFM signals are robust against external interference in underwater acoustic communication, they have limitations in performing additional functions such as CID assignment in channels with severe time–frequency variations, like Doppler effects. Our proposed method uses modified HFM signals (A-HFM) superimposed to simultaneously perform frame detection, frame synchronization estimation, Doppler effect estimation, and CID assignment. The proposed A-HFM-based SA-HFM technique can allocate two-bit information through preamble signal combinations, enabling CID distinction from each matched filter result. This facilitates a stable network configuration in underwater communication and improves communication efficiency for mobile Autonomous Underwater Vehicles (AUVs). To validate our approach, we conducted field experiments in the East Sea of South Korea. The experiments considered various depths (5 m and 100 m) and separation distances (100 m to 2200 m), with the transmitting vessel moving at 1.02–1.54 m/s to simulate Doppler effects in mobile communication environments. The results showed an average SNR above 11 dB, with maximum delay spreads ranging from 0.4 ms to 9.4 ms. The CID assignment performance using the proposed SA-HFM technique achieved over a 93% success rate at separation distances up to 2 km. The Doppler estimation results were consistent with the tone-signal-based estimates, confirming the accuracy of our method. This study demonstrates the possibility of simultaneously performing frame synchronization estimation, Doppler effect estimation, and CID assignment using preamble signals in underwater acoustic communication. The proposed method is highly practical, as it performs multiple functions by modifying existing preamble structures without additional signals or complex algorithms. Future research should focus on the following: Applying the proposed technique in multi-AUV environments to evaluate network scalability. Validating the performance of the method in diverse underwater conditions (e.g., depth variations, currents, noise). Incorporating machine learning and AI algorithms to improve the Doppler effect and channel estimation accuracy. These advancements could enhance the reliability and efficiency of underwater acoustic communication for various applications, including marine exploration, defense, and environmental monitoring. Our results provide new directions for underwater communication system design and implementation, contributing significantly to underwater cellular network development. Continued research and experimentation will further advance underwater acoustic communication technology and expand its applications in marine fields.

Author Contributions: Conceptualization, T.-H.I.; methodology, T.-H.I.; software, S.-Y.P.; validation, T.-H.I. and S.-Y.P.; formal analysis, S.-Y.P. and T.-H.I.; investigation, S.-Y.P. and T.-H.I.; resources, S.-Y.P. and T.-H.I.; data curation, S.-Y.P.; writing—original draft preparation, S.-Y.P.; writing—review and editing, T.-H.I.; visualization, S.-Y.P.; supervision, T.-H.I.; project administration, T.-G.C.; funding acquisition, T.-G.C. All authors have read and agreed to the published version of the manuscript.

Funding: This work was partly supported by Korea Research Institute for Defense Technology Planning and Advancement (KRIT)—Grant funded by Defense Acquisition Program Administration (DAPA), (No. 20-102-B00-007(KRIT-CT-22-085), 70%). This work was also partly supported by the Institute of Information & Communications Technology Planning & Evaluation (IITP)—Innovative Human Resource Development for Local Intellectualization program grant funded by the Korea government (MSIT) (IITP-2025-RS-2024-00436765, 30%).

Data Availability Statement: The raw data supporting the conclusions of this article will be made available by the authors on request.

Conflicts of Interest: Author T.-G.C. was employed by the company LIG Nex1, Seongnam, Republic of Korea. The remaining authors declare that the research was conducted in the absence of any commercial or financial relationship that could be construed as a potential conflict of interest.

References

1. Sahoo, A.; Dwivedy, S.K.; Robi, P.S. Advancements in the field of autonomous underwater vehicle. *Ocean. Eng.* **2019**, *181*, 145–160.
2. Liu, C.; Lv, Z.; Xiao, L.; Su, W.; Ye, L.; Yang, H.; You, X.; Han, S. Efficient Beacon-Aided AUV Localization: A Reinforcement Learning Based Approach. *IEEE Trans. Veh. Technol.* **2024**, *73*, 7799–7811. [CrossRef]
3. Zhu, S.; Han, G.; Lin, C.; Tao, Q. Underwater Target Tracking Based on Hierarchical Software-Defined Multi-AUV Rein-forcement Learning: A Multi-AUV Advantage-Attention Actor-Critic Approach. *IEEE Trans. Mob. Comput.* **2024**, *23*, 13639–13653. [CrossRef]
4. Liu, Y.; Sun, Y.; Li, B.; Wang, X.; Yang, L. Experimental Analysis of Deep-Sea AUV Based on Multi-Sensor Integrated Navigation and Positioning. *Remote. Sens.* **2024**, *16*, 199. [CrossRef]
5. Qiu, T.; Li, Y.; Feng, X. Distributed Channel Sensing MAC Protocol for Multi-UUV Underwater Acoustic Network. *IEEE Internet Things J.* **2024**, *11*, 16119–16133. [CrossRef]
6. Yun, C. Underwater Multi-Channel MAC with Cognitive Acoustics for Distributed Underwater Acoustic Networks. *Sensors* **2024**, *24*, 3027. [CrossRef]
7. Qiao, G.; Babar, Z.; Ma, L.; Liu, S.; Wu, J. MIMO-OFDM underwater acoustic communication systems—A review. *Phys. Commun.* **2017**, *23*, 56–64. [CrossRef]
8. Zhu, J.; Pan, X.; Peng, Z.; Liu, M.; Guo, J.; Zhang, T.; Gou, Y.; Cui, J.-H. A *uw*-Cellular Network: Design, Implementation and Experiments. *J. Mar. Sci. Eng.* **2023**, *11*, 827. [CrossRef]
9. Stojanovic, M.; Preisig, J. Underwater acoustic communication channels: Propagation models and statistical characterization. *IEEE Commun. Mag.* **2009**, *47*, 84–89. [CrossRef]
10. Lee, K.; Kim, J.; Jung, J.; Lee, I. Zadoff-Chu Sequence Based Signature Identification for OFDM. *IEEE Trans. Wirel. Commun.* **2013**, *12*, 4932–4942. [CrossRef]
11. Hyder, M.; Mahata, K. Zadoff–Chu Sequence Design for Random Access Initial Uplink Synchronization in LTE-Like Systems. *IEEE Trans. Wirel. Commun.* **2017**, *16*, 503–511. [CrossRef]
12. Wang, K.; Chen, S.; Liu, C.; Liu, Y.; Xu, Y. Doppler estimation and timing synchronization of underwater acoustic communication based on hyperbolic frequency modulation signal. In Proceedings of the 2015 IEEE 12th International Conference on Networking, Sensing and Control, Taipei, Taiwan, 9–11 April 2015; pp. 75–80. [CrossRef]
13. Kim, Y.J.; Choi, S.J.; Cho, Y.S. Random Access Preamble Design Technique for Non-Terrestrial Networks with High Doppler Shift. *Korean Inst. Commun. Inf. Sci. Conf.* **2023**, *2023*, 716–717. [CrossRef]
14. Kim, Y.J.; Asim, M.; Im, T.H.; Cho, Y.S. Sequence Design Technique for Accurate Timing and Cell ID Estimation in Underwater Acoustic Cellular Systems with a High Doppler. *Electronics* **2021**, *10*, 2413. [CrossRef]
15. Asim, M.; Khan, M.S.; Im, T.H.; Cho, Y.S. Cell ID and Timing Estimation Techniques for Underwater Acoustic Cellular Systems in High-Doppler Environments. *Sensors* **2020**, *20*, 4147. [CrossRef]
16. Wei, R.; Ma, X.; Zhao, S.; Yan, S. Doppler Estimation Based on Dual-HFM Signal and Speed Spectrum Scanning. *IEEE Signal Process. Lett.* **2020**, *27*, 1740–1744. [CrossRef]
17. Zhao, S.; Yan, S.; Xu, L. Doppler Estimation Based on HFM Signal for Underwater Acoustic Time-varying Multipath Channel. In Proceedings of the 2019 IEEE International Conference on Signal Processing, Communications and Computing (ICSPCC), Dalian, China, 20–22 September 2019; pp. 1–6. [CrossRef]
18. Lv, C.; Sun, Q.; Chen, H.; Xie, L. Doppler and Channel Estimation Using Superimposed Linear Frequency Modulation Preamble Signal for Underwater Acoustic Communication. *J. Mar. Sci. Eng.* **2024**, *12*, 338. [CrossRef]
19. Kim, M.-S.; Im, T.-H.; Cho, Y.-H.; Kim, K.-W.; Ko, H.-L. HFM design for timing synchronization in underwater communications systems. In Proceedings of the OCEANS 2017—Aberdeen, Aberdeen, UK, 19–22 June 2017; pp. 1–4. [CrossRef]

20. Ling, Z.; Xie, L.; Chen, H. Joint Doppler Scale Estimation and Timing Synchronization in Underwater Acoustic Communications. In Proceedings of the 2019 IEEE International Conference on Signal Processing, Communications and Computing (ICSPCC), Dalian, China, 20–22 September 2019; pp. 1–6. [CrossRef]
21. Zuberi, H.H.; Liu, S.; Sohail, M.Z.; Pan, C. Multi-user underwater acoustic communication using binary phase-coded hyperbolic frequency-modulated signals. *IET Commun.* **2022**, *16*, 1415–1427. [CrossRef]
22. Qu, Z.; Lai, M. A Review on Electromagnetic, Acoustic, and New Emerging Technologies for Submarine Communication. *IEEE Access* **2024**, *12*, 12110–12125. [CrossRef]
23. Kilfoyle, D.; Baggeroer, A. The state of the art in underwater acoustic telemetry. *IEEE J. Ocean. Eng.* **2000**, *25*, 4–27. [CrossRef]
24. Sozer, E.; Stojanovic, M.; Proakis, J. Underwater acoustic networks. *IEEE J. Ocean. Eng.* **2000**, *25*, 72–83. [CrossRef]
25. Ko, H.; Lee, H.; Cha, M.; Kim, S.; Kim, S.; Im, T. Base Station-based Underwater Communication Network. In Proceedings of the OCEANS 2023—Limerick, Limerick, Ireland, 5–8 June 2023; pp. 1–5. [CrossRef]
26. Yoon, S.; Azad, A.K.; Oh, H.; Kim, S. AURP: An AUV-Aided Underwater Routing Protocol for Underwater Acoustic Sensor Networks. *Sensors* **2012**, *12*, 1827–1845. [CrossRef] [PubMed]
27. Stefanov, A.; Stojanovic, M. Design and Performance Analysis of Underwater Acoustic Networks. *IEEE J. Sel. Areas Commun.* **2011**, *29*, 2012–2021. [CrossRef]
28. Liu, Y.; Wang, H.; Cai, L.; Shen, X.; Zhao, R. Fundamentals and Advancements of Topology Discovery in Underwater Acoustic Sensor Networks: A Review. *IEEE Sens. J.* **2021**, *21*, 21159–21174. [CrossRef]
29. Li, W.; Zhou, S.; Willett, P.; Zhang, Q. Preamble Detection for Underwater Acoustic Communications Based on Sparse Channel Identification. *IEEE J. Ocean. Eng.* **2019**, *44*, 256–268. [CrossRef]
30. Arab, H.; Dufour, S.; Moldovan, E.; Akyel, C.; Tatu, S.O. Accurate and Robust CW-LFM Radar Sensor: Transceiver Front-End Design and Implementation. *IEEE Sens. J.* **2019**, *19*, 1943–1950. [CrossRef]
31. Huang, S.; Fang, S.; Han, N. An Improved Velocity Estimation Method for Wideband Multi-Highlight Target Echoes in Active Sonar Systems. *Sensors* **2018**, *18*, 2794. [CrossRef]
32. Lee, D.-H.; Shin, J.-W.; Do, D.-W.; Choi, S.-M.; Kim, H.-N. Robust LFM Target Detection in Wideband Sonar Systems. *IEEE Trans. Aerosp. Electron. Syst.* **2017**, *53*, 2399–2412. [CrossRef]
33. Knight, W.; Pridham, R.; Kay, S. Digital signal processing for sonar. *Proc. IEEE* **1981**, *69*, 1451–1506. [CrossRef]
34. Sun, Q.; Wu, F.-Y.; Yang, K.; Ma, Y. Estimation of multipath delay-Doppler parameters from moving LFM signals in shallow water. *Ocean Eng.* **2021**, *232*, 109125. [CrossRef]
35. Cui, X.; Yan, P.; Li, J.; Zhang, H.; Li, S.; Liu, J. Timing estimation of multiple hyperbolic frequency-modulated signals based on multicarrier underwater acoustic communication. *Trans. Emerg. Telecommun. Technol.* **2022**, *33*, e4636. [CrossRef]
36. Zhou, W.; Yeh, C.-M.; Jin, K.; Yang, J.; Lu, Y.-B. ISAR Imaging Based on the Wideband Hyperbolic Frequency-ModulationWaveform. *Sensors* **2015**, *15*, 23188–23204. [CrossRef] [PubMed]
37. Wang, Y.; Dong, X. Comparison of Frequency Offset and Timing Offset Effects on the Performance of SC-FDE and OFDM Over UWB Channels. *IEEE Trans. Veh. Technol.* **2009**, *58*, 242–250. [CrossRef]